Biochimica et Biophysica Acta 1847 (2015) 709–716

Contents lists available at ScienceDirect

Biochimica et Biophysica Acta

journal homepage: www.elsevier.com/locate/bbabio

A T67A mutation in the proximal pocket of the high-spin heme of MauG stabilizes formation of a mixed-valent Fe^{II}/Fe^{III} state and enhances charge resonance stabilization of the *bis*-Fe^{IV} state ☆

Sooim Shin [a], Manliang Feng [b], Chao Li [c], Heather R. Williamson [d], Moonsung Choi [e], Carrie M. Wilmot [c], Victor L. Davidson [d,*]

[a] Department of Bioengineering and Biotechnology, College of Engineering, Chonnam National University, Chonnam, South Korea
[b] Department of Chemistry, Tougaloo College, Tougaloo, MS 39174, USA
[c] Department of Biochemistry, Molecular Biology and Biophysics, University of Minnesota, St. Paul, MN 55108, USA
[d] Burnett School of Biomedical Sciences, College of Medicine, University of Central Florida, Orlando, FL 32827, USA
[e] Department of Optometry, College of Energy and Biotechnology, Seoul National University of Science and Technology, Seoul 139-743, South Korea

ARTICLE INFO

Article history:
Received 17 February 2015
Received in revised form 3 April 2015
Accepted 12 April 2015
Available online 17 April 2015

Keywords:
Charge–resonance-transition
Cytochrome
Electron transfer
Ferryl
Heme
Metalloprotein

ABSTRACT

The diheme enzyme MauG catalyzes a six-electron oxidation required for posttranslational modification of a precursor of methylamine dehydrogenase (preMADH) to complete the biosynthesis of its protein-derived tryptophan tryptophylquinone (TTQ) cofactor. One heme is low-spin with ligands provided by His205 and Tyr294, and the other is high-spin with a ligand provided by His35. The side chain methyl groups of Thr67 and Leu70 are positioned at a distance of 3.4 Å on either side of His35, maintaining a hydrophobic environment in the proximal pocket of the high-spin heme and restricting the movement of this ligand. Mutation of Thr67 to Ala in the proximal pocket of the high-spin heme prevented reduction of the low-spin heme by dithionite, yielding a mixed-valent state. The mutation also enhanced the stabilization of the charge–resonance-transition of the high-valent *bis*-Fe^{IV} state that is generated by addition of H_2O_2. The rates of electron transfer from TTQ biosynthetic intermediates to the high-valent form of T67A MauG were similar to that of wild-type MauG. These results are compared to those previously reported for mutation of residues in the distal pocket of the high-spin heme that also affected the redox properties and charge resonance transition stabilization of the high-valent state of the hemes. However, given the position of residue 67, the structure of the variant protein and the physical nature of the T67A mutation, the basis for the effects of the T67A mutation must be different from those of the mutations of the residues in the distal heme pocket.

1. Introduction

The biosynthesis of the protein-derived cofactor [1,2], tryptophan tryptophylquinone (TTQ) [3] in methylamine dehydrogenase (MADH) [4] requires MauG, a 42 kDa *c*-type diheme enzyme [5]. In order to complete TTQ formation, MauG catalyzes a series of posttranslational modifications that result in a six-electron oxidation of a precursor of methylamine dehydrogenase (preMADH) that possesses a monohydroxylated residue βTrp57 [6,7] (Fig. 1). The order of the reactions that MauG catalyzes are (i) covalent crosslinking of βTrp57 to βTrp108, (ii) insertion of a second oxygen atom into the side-chain of βTrp57, and (iii) oxidation of the quinol species to the quinone [8]. MauG-dependent TTQ biosynthesis requires long-range interprotein electron transfer (ET). In the crystal structure of a catalytically competent complex of MauG and preMADH from *Paracoccus denitrificans* the distances between the residues of preMADH that are modified to form TTQ and each heme iron of MauG are 40.1 and 19.4 Å, respectively [9]. Site-directed mutagenesis, and kinetic and thermodynamic analyses showed that the long range ET that is required for catalysis involves a hole-hopping mechanism that is mediated by Trp199 of MauG [10,11].

The two ferric hemes of MauG are present in different spin states [12]; a high-spin five-coordinate heme that is ligated by His35 and a low-spin six-coordinate heme with two protein ligands provided by His205 and Tyr294 [9]. The redox properties of MauG are distinct from other diheme proteins [13]. During inter-conversions between the

Abbreviations: TTQ, tryptophan tryptophylquinone; MADH, methylamine dehydrogenase; preMADH, the biosynthetic precursor protein of MADH with incompletely synthesized TTQ; *bis*-Fe(IV) MauG, redox state of MauG with one heme as Fe(IV)═O and the other as Fe(IV); ET, electron transfer; WT, wild-type; E_m, oxidation–reduction midpoint potential; NIR, near infrared

☆ Coordinates and structure factors for the T67A MauG–preMADH complex have been deposited in the Protein Data Bank as 4Y5R.

* Corresponding author at: Burnett School of Biomedical Sciences, College of Medicine, University of Central Florida, 6900 Lake Nona Blvd., Orlando, FL 32827, USA. Tel.: +1 407 266 7111; fax: +1 407 266 7002.
E-mail address: victor.davidson@ucf.edu (V.L. Davidson).

http://dx.doi.org/10.1016/j.bbabio.2015.04.008
0005-2728/

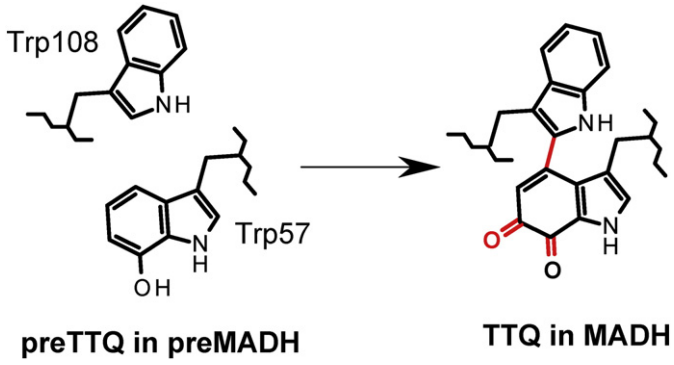

Fig. 1. MauG catalyzed TTQ biosynthesis from preMADH. The posttranslational modifications of preMADH which are catalyzed by MauG are highlighted in red.

diferric and diferrous states, the two hemes are oxidized and reduced simultaneously suggesting that they have similar oxidation–reduction midpoint potential (E_m) values for the Fe^{III}/Fe^{II} redox couple. A mixed-valent state in which one heme is ferric and the other is ferrous was not observed. However, spectrochemical redox titration of MauG yielded two E_m values of −159 and −254 mV which describe the sequential addition or removal of one electron to or from the diheme system. This phenomenon was assigned to redox cooperativity between the two hemes [14]. Furthermore, oxidation of diferric MauG by H_2O_2 or diferrous MauG by O_2 generates a novel high-valent *bis*-Fe^{IV} state of MauG [15] in which the high-spin heme is present as Fe^{IV}═O with the His35 ligand, and the other heme is present as Fe^{IV} with the His–Tyr axial ligation retained [9]. This *bis*-Fe^{IV} species, which is required for TTQ biosynthesis, is stabilized by an unusual charge–resonance transition in which the two Fe^{IV} hemes and Trp93, which resides between the two hemes, share charge and spin via hopping-mediated ultrafast ET [16].

MauG has been the subject of several studies in which site-directed mutagenesis of residues in the diheme site (Fig. 2) were used to elucidate structure–function relationships. Roles in stabilization of the *bis*-Fe^{IV} state and TTQ biosynthesis activity have been described for the Tyr294 ligand of the six-coordinate heme, and Trp93 which resides between the two hemes [17–21]. Three residues in the distal pocket of the high-spin five-coordinate heme were also examined. Pro107 was shown to be critical in maintaining the proper structure of the distal pocket of the high-spin heme, controlling the binding of exogenous ligands, directing the reactivity of the heme-activated oxygen, and minimizing the deleterious oxidation of other residues of MauG [22,23]. Mutation of Gln103 significantly affected the overall protein stability of MauG and altered the redox properties of the hemes [24]. The carboxyl group of Glu113 was shown to be an important determinant of the distribution of high-valent species that participate in charge–resonance stabilization of the *bis*-Fe^{IV} redox state, as well as in the maintenance of the redox cooperativity between the two hemes of MauG [25].

This study is the first to examine the importance of a residue in the proximal heme pocket of the high-spin heme of MauG. Typically hemes that react with O_2 or H_2O_2 exhibit hydrogen-bonding interactions between the conserved proximal His ligand and neighboring residues. These hydrogen bonds are believed to stabilize the Fe^{IV} state of the heme. MauG is distinct from these other heme proteins in that the proximal His35 ligand of its high-spin heme is surrounded by hydrophobic residues. Side chain methyl groups of two residues, Thr67 and Leu70, are positioned at a distance of 3.4 Å on either side of the His35 ligand, maintaining a hydrophobic environment and restricting the movement of the His35 side-chain. In this study it is shown that replacement of Thr67 with Ala significantly alters the redox properties of the hemes of MauG and nature of the high-valent state of the diheme system in ways that have not been seen for previous site-directed mutations of MauG.

2. Materials and methods

2.1. Protein expression and purification

Recombinant MauG [5] and preMADH [6] were purified from *P. denitrificans* and *Rhodobacter sphaeroides*, respectively, as described previously. Thr67 of MauG was converted to Ser and Ala by site-directed mutagenesis of double-stranded pMEG391, which contains *mau*G, using the Phusion site-directed mutagenesis kit (New England Bio Lab). The recombinant MauG variant proteins were homologously expressed in *P. denitrificans* and isolated from the periplasmic fraction as described for recombinant wild-type (WT) MauG [5].

2.2. Redox titrations

E_m values of T67A MauG were determined by anaerobic spectrochemical titrations, as described previously for WT MauG using FMN as a mediator [26] and sodium dithionite and potassium ferricyanide as reductant and oxidant, respectively. The fraction of MauG that was reduced was determined by comparison with the spectra of the

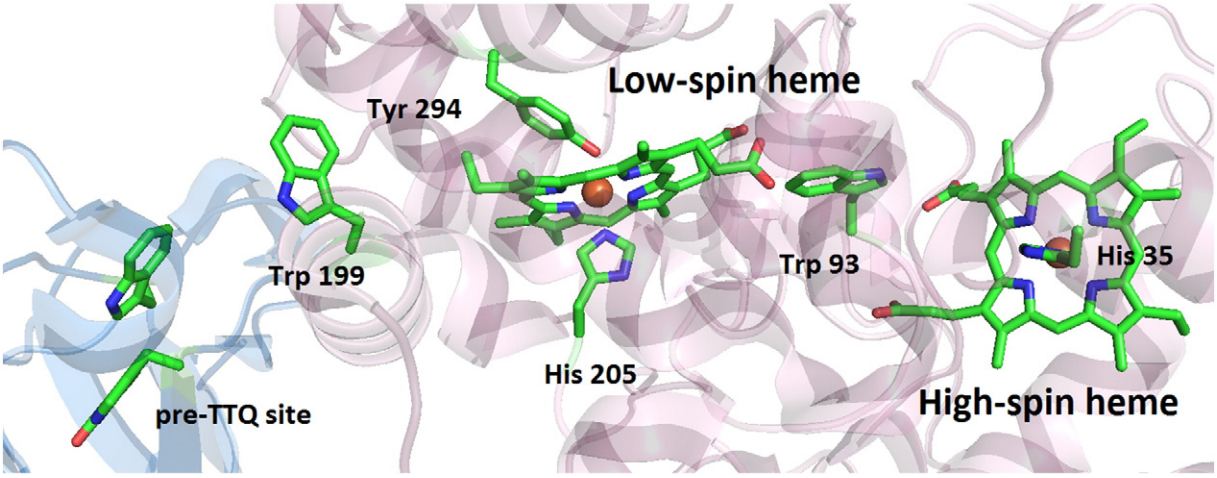

Fig. 2. Structure of the diheme site of MauG. The MauG is shown in pink ribbon and the preMADH as blue ribbon. The hemes and key residues involved in the maturation of MADH are drawn in atoms colors (carbon, green), and irons are drawn as orange spheres. This figure was produced from PDB ID: 3L4M (the MauG–preMADH complex) using PyMOL (http://www.pymol.org/).

completely oxidized and reduced forms of MauG and quantitated from the absorbance at 550 nm. Data were fit to Eq. (1), which describes the redox behavior of a system with a single redox-active center, and Eq. (2), which describes the redox behavior of a system with two redox active centers, where a is the fraction of the total absorbance change attributable to one center and $(1 - a)$ is the fraction of the total absorbance change attributable to the other.

$$E = E_m + (2.3RT/nF)\ \log([\mathrm{MauG_{oxi}}]/[\mathrm{MauG_{red}}]). \quad (1)$$

$$\text{Fraction reduced} = a\Big/\left[1 + 10^{((E\text{-}Em1)/0.059\ \mathrm{V})}\right] + (1\text{-}a)\Big/\left[1 + 10^{((E\text{-}Em2)/0.059\ \mathrm{V})}\right]. \quad (2)$$

2.3. Resonance Raman spectroscopy

Resonance Raman spectra were recorded using a Raman spectrometer consisting of a Spex model 1877 triple spectrograph and a CCD detector as reported previously [26]. A 406.7 nm line from an argon–krypton ion laser (Spectra-Physics BeamLok model 2080-KV) was used as the excitation source, and the Raman signal was collected in a 120° geometry. The laser power was adjusted to ~5 mW at the sample. Each spectrum was recorded with a 60 s accumulation time, and 10 repetitively measured spectra were averaged to improve the quality of the final spectrum. The frequencies of the Raman bands were calibrated using the standard spectrum of cyclohexane. Samples contained 0.15 mM protein in 50 mM potassium phosphate buffer, pH 7.5, and spectra were recorded at 25 °C.

2.4. Electron transfer reactions to bis-Fe^{IV} MauG

The single-turnover kinetics of the reactions of preMADH and quinol MADH with *bis*-Fe^{IV} MauG were studied as described previously [27] using an On-line Instrument Systems (OLIS, Bogart, GA) RSM stopped-flow spectrophotometer. Kinetic data collected in the rapid-scanning mode were globally fit using the fitting routines of OLIS Global Fit. Each reaction was performed in 10 mM potassium phosphate buffer, pH 7.5, at 25 °C. Each reaction mixture contained 2.0 μM of the limiting reactant, either WT or T67A *bis*-Fe^{IV} MauG, which was generated with a substoichiometric concentration of H_2O_2 to ensure that excess unreacted H_2O_2 was not present after *bis*-Fe^{IV} formation. Saturating concentrations of the substrates were used; either 8 μM preMADH or 35 μM quinol MADH.

2.5. Crystallization and X-ray structure determinations of the T67A MauG—preMADH complex

To crystallize the T67A MauG—preMADH complex, the proteins were added in a 2:1 ratio to give a protein solution containing 68 μM for T67A MauG, 34 μM for preMADH, 100 mM NaCl, 50 mM potassium phosphate buffer, pH 7.5. The protein solution was centrifuged at 13,400 rpm for 30 min prior to setting up the crystallization experiment. Crystallization conditions were similar to those of WT MauG/preMADH using hanging drop vapor diffusion [9]; the reservoir solution contained 26–30% PEG 8000, 0.1 M sodium acetate, 0.1 M MES, pH 6.4. To obtain diffracting crystals, 1 μL of protein solution was mixed with 3 μL of reservoir solution. Crystals appeared after 2 days, and grew to full size in 3 weeks. Crystals were cryo-protected in artificial mother liquor containing reservoir solution and 10% PEG 400.

Diffraction data were collected at 100 K, on GM/CA beamline 23-ID-B of the Advanced Photon Source (APS), Argonne National Laboratory, Argonne, IL. The diffraction data are isomorphous with those of the triclinic WT MauG—preMADH complex [9]. Data were processed by XDS [28], and the structure was solved by difference Fourier. The model used for phasing was the WT MauG—preMADH structure (PDB ID: 3L4M) with solvent and ligands removed. Restrained refinement was performed with Refmac5 [29] in the CCP4 program suite [30], and model building was conducted in Coot [31].

3. Results

3.1. Protein expression

Thr67 was converted to Ser and Ala by site-directed mutagenesis. T67S MauG was not detected in the expression system. This suggests that this mutation either disrupted the biosynthesis of MauG or decreased its stability, or both. T67A MauG was expressed; however, the yield of the purified protein was typically two to five-fold less than that of recombinant WT MauG.

3.2. X-ray crystal structure of the T67A MauG—preMADH complex

The overall structure of the T67A MauG—preMADH complex was very similar to that of the WT MauG—preMADH complex [9], although the resolution was only to 2.8 Å compared to 2.1 Å for the WT complex (Table 1). Crystals of equivalent size to those of the WT MauG—preMADH complex could not be obtained for the T67A MauG—preMADH complex even with seeding, and this may explain the lower resolution. The mutation of Thr67 to Ala was clearly observed in the $2F_o - F_c$ electron density and $F_o - F_c$ difference map (Fig. 3A). Other residues in the proximal and distal pockets of the high spin heme were not perturbed by the mutation, within error (Fig. 3B). As such, the structural environment around the high-spin heme was maintained, although at this resolution the presence of structured water in the absence of the Thr side-chain cannot be ruled out.

Table 1
X-ray crystallography data collection and refinements statistics[a].

Data collection	
Space group	P1
Unit cell lengths (Å)	55.53 × 83.52 × 107.78
Unit cell angles (°)	109.94 × 91.54 × 105.78
Wavelength (Å)	1.003317
Resolution (Å)[a]	29.66–2.80 (2.89–2.80)
Completeness (%)[a]	93.6 (98.1)
Measured reflections	98,679
Unique reflections	39,896
Rmerge (%)[a,b]	11.9 (20.9)
I/σI[a]	5.2 (1.9)
Multiplicity[a]	1.9 (1.9)
Refinement	
R_{work}[c]	0.1937
R_{free}[d]	0.2564
Protein atoms	13,299
Ligand atoms	121
Solvent atoms	6
Ramachandran statistics[e]	
Allowed	99.00%
Outlier	1.00%
Root mean square deviation	
Bond lengths (Å)	0.0109
Bond angles (°)	1.7098
Average B factor (Å^2)	38.51
Protein data bank ID	4Y5R

[a] Values in parentheses are for the highest resolution shell.
[b] $R_{merge} = \Sigma_i\ |I_{hkl,i} - \langle I_{hkl}\rangle|/\Sigma_{hkl}\ \Sigma_i\ I_{hkl,i}$, where I is the observed intensity and $\langle I_{hkl}\rangle$ is the average intensity of multiple measurements.
[c] $R_{work} = \Sigma||F_o| - |F_c||/\Sigma|F_o|$, where $|F_o|$ is the observed structure factor amplitude, and $|F_c|$ is the calculated structure factor amplitude.
[d] R_{free} is the R factor based on 5% of the data excluded from refinement.
[e] Based on values attained from refinement validation options in COOT.

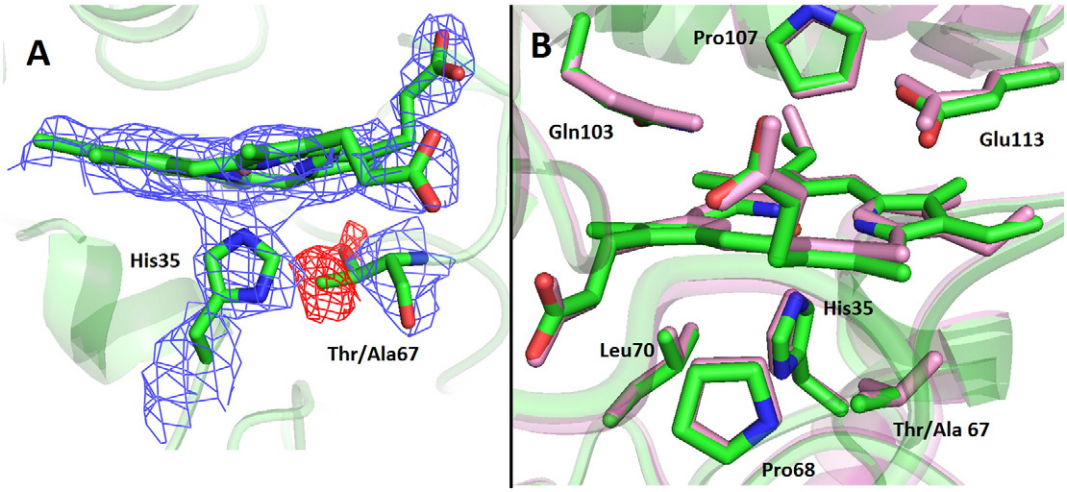

Fig. 3. Crystal structure of T67A MauG–preMADH complex. (A) Electron density at the T67A mutation site. Negative $F_o - F_c$ electron density shown as red mesh contoured at -3σ from phasing with WT MauG–preMADH model (green, PDB ID: 3L4M). $2F_o - F_c$ electron density shown as blue mesh contoured at 1σ. (B) Overlay of the high-spin heme proximal pocket of WT MauG (pink) and T67A MauG (green)–preMADH crystals. Hemes and residues of interest are drawn in sticks colored by atom, with the remaining protein shown in cartoon. The iron is displayed as an orange sphere. This figure was produced from PDB ID: 3L4M (the MauG–preMADH complex) using PyMOL (http://www.pymol.org/).

3.3. Effects of the T67A mutation on the spectroscopic properties of the oxidized and reduced forms of MauG

The absorbance spectrum of diferric T67A MauG is similar to that of WT MauG except for a 2 nm blue shift of the Soret peak maximum and a slight broadening of the Soret peak (Fig. 4). Anaerobic reductive titration of WT MauG with dithionite requires two electron equivalents and yields the spectrum of the diferrous enzyme with an increase in intensity and red shift of the Soret peak to 418 nm with a shoulder at 427 nm, and appearance of the α and β bands at 550 nm and 524 nm, respectively [5]. In contrast, the spectral changes of T67A MauG that resulted from addition of dithionite were complete after addition of only one electron equivalent and further addition of dithionite resulted in no additional spectral changes. The resulting spectrum (Fig. 4) was different than that of fully reduced WT MauG and exhibited a small Soret peak shift to 412 nm without an increase in intensity and with a more pronounced shoulder at 427 nm. The α and β bands were not well resolved. These results are consistent with a mixed-valent state in which only one heme has been reduced. A mixed-valent state was not observed for WT MauG, or all but one of the many other variant MauG proteins which have been previously studied [7,10,17,18,22,26]. The exception is E113Q MauG, which like T67A MauG could only be reduced by dithionite to a mixed-valent state which exhibited an absorbance spectrum very similar to that of T67A MauG [25].

It is difficult to distinguish the spin states of the hemes by absorbance spectroscopy. However, bands in the resonance Raman spectrum are sensitive to oxidation state and spin state [32–34]. The resonance Raman spectra of diferric WT MauG and T67A MauG are essentially identical (Fig. 5). In each, the oxidation state marker band (ν_4) is centered at 1374 cm^{-1} indicating that both hemes are in the ferric state. Each spectrum contains ν_3 bands at 1478^{-1} and 1501 cm^{-1}, which correspond to the high-spin and low-spin hemes, respectively. After addition of dithionite, the spectra of WT MauG and T67A MauG were different (Fig. 5). The spectrum of WT MauG shows a single ν_4 band that is centered at 1359 cm^{-1} indicating that both hemes are in the ferrous state and the ν_3 bands have shifted to 1467^{-1} and 1492 cm^{-1} for the high-spin and low-spin hemes, respectively. In contrast, the spectrum of T67A MauG shows two ν_4 bands of approximately equal intensity centered at 1359 cm^{-1} and 1374 cm^{-1}, indicating that one heme is Fe^{III} and one is Fe^{II}. The ν_3 band for the high-spin heme exhibits the same shift as seen in the WT MauG spectrum indicating that it is the ferrous heme. The position of the ν_3 band for the low-spin heme at 1501 cm^{-1} indicates that it is still ferric. These results indicate that the absorption spectrum of dithionite-reduced T67A MauG in Fig. 4B is indeed that of a mixed-valent state with the high-spin heme as Fe^{II} and the low-spin heme as Fe^{III}. Addition of CO to the dithionite-reduced T67A MauG resulted in changes in the resonance Raman spectrum which indicated that CO did bind to the high-spin ferrous heme iron. This indicates that the mutation did not affect the accessibility of the high-spin heme to external ligands.

3.4. Effect of the T67A mutation on the E_m values of MauG

Spectrochemical titrations of T67A MauG yielded linear plots that fit well to Eq. (1) and yielded an E_m value of -158 ± 1 mV and an n value of 1.16 ± 0.04 (Fig. 6). Fitting the data to Eq. (2) also yielded only a

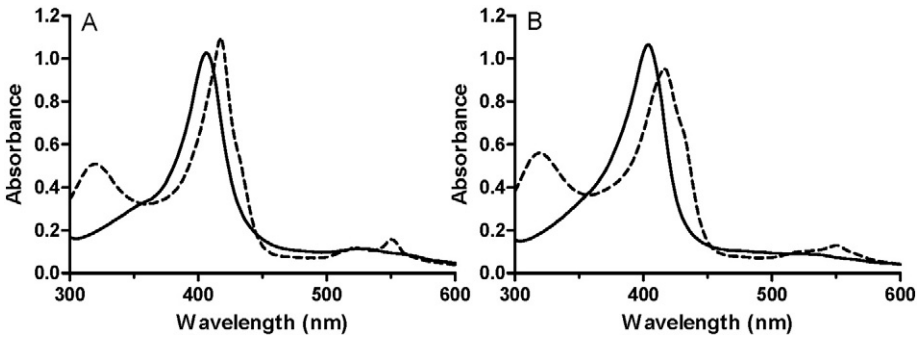

Fig. 4. Absorption spectra of WT MauG (A) and T67A MauG (B). A) Spectra are overlaid of 2 μM diferric protein before (solid line) and after (dashed line) reduction by sodium dithionite.

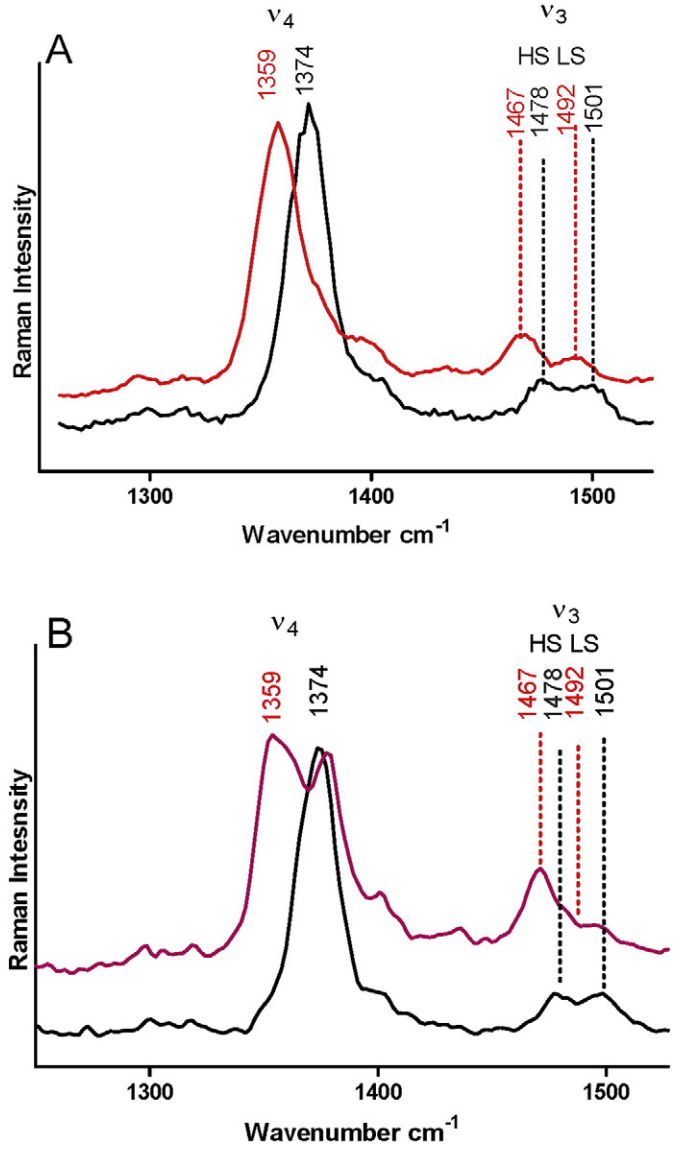

Fig. 5. Resonance Raman spectra of oxidized and reduced WT MauG (A) and T67A MauG (B). Spectra are overlaid of the diferric protein before (black line) and after reduction by dithionite (red line). Marker bands and their frequencies are indicated. HS and LS refer to high-spin and low-spin heme.

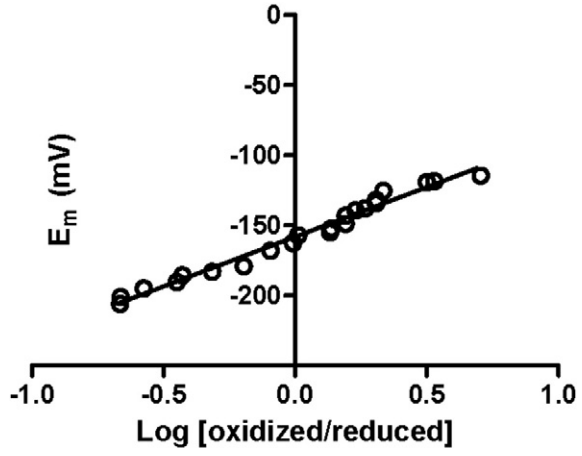

Fig. 6. Spectrochemical redox titration of T67A MauG. The solid line is the fit of the data by Eq. (1).

single value of −158 mV indicating that the two-component model was inappropriate. These results are consistent with only a single heme in T67A MauG being reduced. This is in contrast to WT MauG which exhibits two E_m values of −158 mV and −246 mV that correspond to the sequential addition or removal of the first and second electrons to or from the diheme system, respectively [26]. It is noteworthy that E113Q MauG, which also could only be reduced to the mixed valent state, also yielded a single E_m value. However, that value was −196 mV [25].

3.5. Effects of the T67A mutation on the reaction of MauG with H_2O_2

Reaction of diferric WT MauG with stoichiometric H_2O_2 results in the formation of a *bis*-Fe^{IV} redox state [15] which is accompanied by changes in the absorbance spectrum (Fig. 7). In the visible spectrum one observes a decrease in intensity and shift of the Soret peak from 406 nm to 408 nm and appearance of minor peaks at 526 and 559 nm [16,27]. In the near infrared (NIR) absorbance spectrum an absorption feature appears which exhibits a maximum at 950 nm. This absorbance at 950 nm has been attributed to a charge–resonance-transition phenomenon, involving the two hemes and the intervening Trp93 residue, which stabilizes the *bis*-Fe^{IV} state [16]. These spectral changes form very quickly ($k > 300\ s^{-1}$) [27] and subsequently return over several minutes to the spectrum of the diferric MauG. Very similar spectral changes were observed after reaction of T67A MauG with stoichiometric H_2O_2. However, the magnitude of change at the Soret region for T67A MauG was greater than that of WT (Fig. 7). The rates of return to the starting spectrum (Fig. 7E) in the Soret region were similar; $0.167 \pm 0.004\ min^{-1}$ for T67A MauG and $0.152 \pm 0.010\ min^{-1}$ for WT MauG. The magnitude of change of the NIR absorbance feature at 950 nm for T67A MauG was similar for WT MauG, however; the rate of decay was much slower for T67A MauG (Fig. 7F).

3.6. Effects of the T67A mutation on electron transfer reactions of bis-Fe^{IV} MauG

It is possible to study two ET reactions involving the *bis*-Fe^{IV} state of MauG using single-turnover kinetics [27,35]. The reaction with preMADH is the first step in the six-electron oxidation reaction of MauG-dependent TTQ biosynthesis and the reaction with quinol MADH is the last step in overall reaction. The reactions with saturating concentrations of preMADH yielded rate constants of $0.54 \pm 0.05\ s^{-1}$ for WT MauG and $0.45 \pm 0.08\ s^{-1}$ for T67A MauG. The reactions with saturating concentrations of quinol MADH yielded rate constants of $20.5 \pm 2.3\ s^{-1}$ for WT MauG and $16.4 \pm 1.8\ s^{-1}$ for T67A MauG. Thus, the T67A mutation has had little effect on these two ET reactions involving the *bis*-Fe^{IV} state of the diheme enzyme.

4. Discussion

A distinguishing feature of MauG is that it possesses two hemes that are physically separated yet function as a single two-electron diheme redox center [13,36]. During the interconversion between the diferric and diferrous states the two hemes reduce and oxidize simultaneously but exhibit two E_m values that are associated with this redox couple because of redox cooperativity between the hemes [26]. A mixed-valence state is not observed. Similarly the interconversion of the two hemes from the diferric state to the *bis*-Fe^{IV} state occurs simultaneously [15]. The formation and relatively long lifetime of this *bis*-Fe^{IV} state are a consequence of charge–resonance-transition [16] that is achieved through ultrafast ET between hemes that is mediated by the intervening Trp93 residue. In this model the *bis*-Fe^{IV} state is the dominant species, but is part of an ensemble of resonance structures including compound ES-like and compound I-like forms of the high-spin heme [16].

The observation that only the high-spin heme of T67A MauG was reduced by dithionite suggests that the T67A mutation has caused the

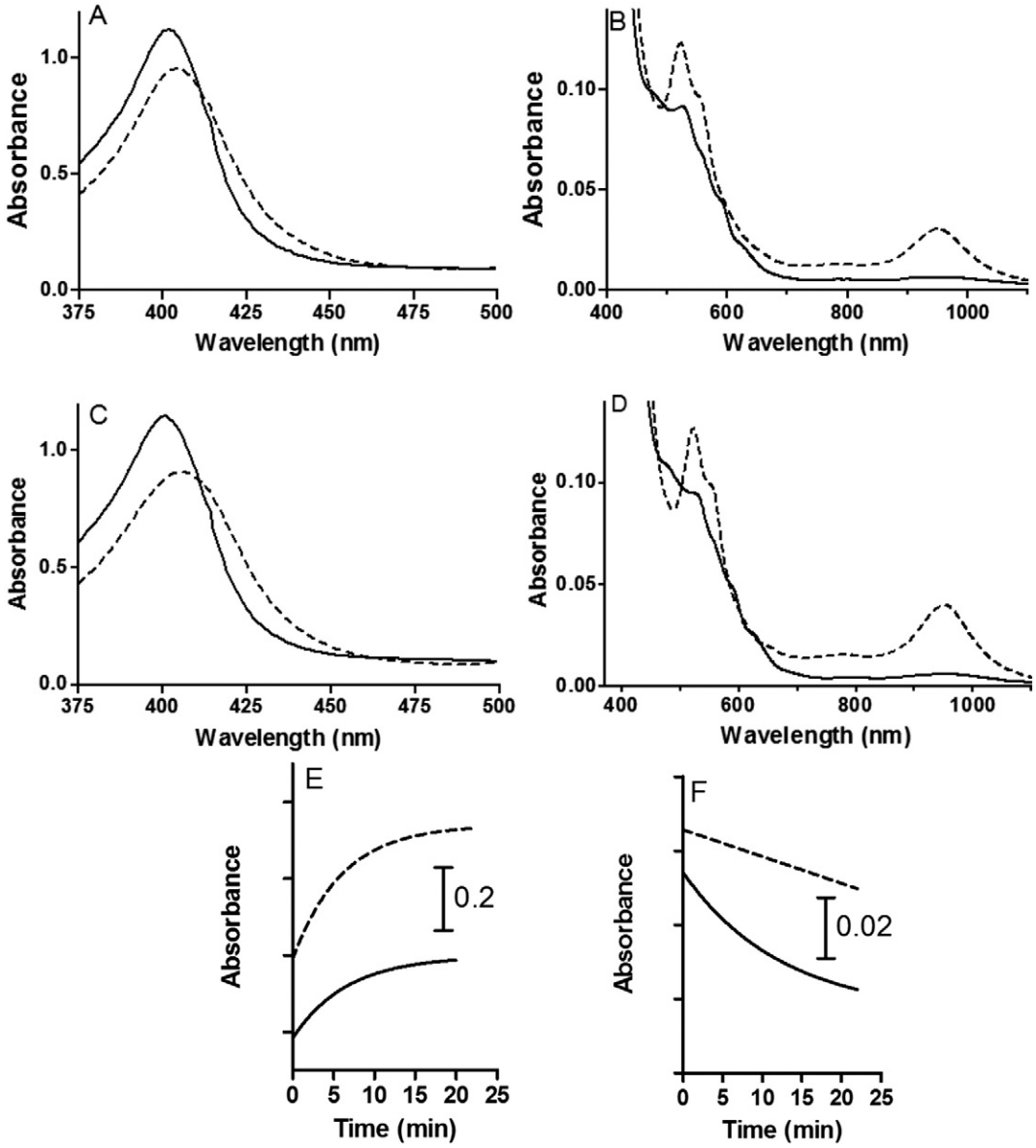

Fig. 7. Visible absorption spectra of diferric WT MauG and T67A MauG before and after addition of H_2O_2. Spectra are overlaid of the Soret regions of the spectra of WT MauG (A) and T67A (C), and the higher wavelength and NIR regions of the spectra of WT MauG (B) and T67A (D), before (solid line) and after (dashed line) addition of a stoichiometric amount of H_2O_2. The time courses for the reversal of the spectral changes at 405 nm (E) and 950 nm (F) that were caused by addition of H_2O_2 are shown for WT (solid line) and T67A MauG (dashed line).

E_m value of the low-spin heme to become more negative than that of dithionite. Not only would this be an unusually negative E_m value for a heme iron, but also it is not evident how mutation of a residue in the proximal pocket of the high-spin heme would alter the E_m value of the low-spin heme. It was previously shown that an E113Q mutation disrupted the redox cooperativity of the Fe^{II}/Fe^{III} redox couple in MauG and this variant could also only be reduced by one electron to a mixed-valent state [25]. Since the only significant structural difference caused by that mutation was the loss of a negative charge in the distal pocket of the high-spin heme, it was suggested that this change prevented the low-spin heme from being reduced by dithionite. A similar result is observed with the T67A mutation, although this mutation does not alter the electrostatic environment of the distal heme pocket. Thus, the mechanistic basis for the disruption of the redox cooperativity in T67A MauG must be different from that postulated for E113Q MauG.

Whereas the effects of the T67A mutation on the spectroscopic and redox properties of the oxidized and reduced forms of MauG were similar to those caused by the E113Q mutation, the effects on the reaction with H_2O_2 were quite different [25]. With E113Q MauG only a small red shift of the left side of the Soret peak was observed upon oxidation and the two new peaks at 526 and 559 nm observed in WT and T67A MauG were absent. However, the NIR absorbance feature at 950 nm was observed for E113Q MauG, but with a weaker intensity. Furthermore, its rate of formation was much slower (~4 s) than observed for WT MauG and the rate of decay was faster. With T67A MauG the spectral changes caused by addition of H_2O_2 were qualitatively similar to WT MauG with increased intensity, and while the rate of the spontaneous reversal of the spectral changes in the Soret region was similar to WT MauG, the rate of decay of the absorbance at 950 nm was much slower. It should be noted that the 950 nm peak in the NIR spectrum derives from a charge–resonance-transition phenomenon that is correlated with an ensemble of resonance structures that includes *bis*-Fe^{IV}. Thus, the magnitude of this peak does not necessarily correlate with the proportion of *bis*-Fe^{IV} (or any one resonance structure) within the ensemble. Thus, it appears that the T67A mutation has stabilized the charge–resonance-transition of the diheme site, whereas the previous E113Q mutation destabilized it.

A consequence of the charge–resonance-transition model for *bis*-Fe^{IV} stabilization in MauG [16] is that replacement of amino acid residues in close proximity to either heme may influence the distribution of the resonance structures. It was proposed that the E113Q MauG mutation altered the distribution of resonance structures such that the *bis*-Fe^{IV} state was no longer the dominant species. As such, the unfavorable resonance equilibrium for *bis*-Fe^{IV} stabilization limited the availability of the *bis*-Fe^{IV} species, thus reducing the rate of its reaction with substrate. These results may also be compared to those caused by mutation of Gln103, another residue in the distal pocket of the high-spin heme (see Fig. 3). Q103N MauG retained the redox cooperativity of the hemes and spectroscopic features of the *bis*-Fe^{IV} state after addition of H_2O_2. However in this case, the rate of the reversal of the spectral changes in the Soret region was 4.5-fold greater than for WT MauG while the rate of decay of the absorbance at 950 nm was similar to WT MauG. The results obtained for Q103N MauG further suggested that as a consequence of the mutation of this residue in the distal heme pocket, a different distribution of resonance structures stabilizes the *bis*-Fe^{IV} state.

4.1. Summary

The results with T67A MauG are distinct from previous studies. This is the first study that shows that mutation of a residue on the proximal side of the high-spin heme can affect the distribution and stabilization of resonance forms of the high-valent state of MauG, in addition to disrupting the redox cooperativity of the diferric/diferrous redox couple. Furthermore, with T67A MauG the charge–resonance-stabilization is longer lasting as evidenced by the much slower decay of the 950 nm absorbance. Initially, after H_2O_2 addition to T67A MauG it appears that the *bis*-Fe^{IV} state is the dominant resonance species. The spontaneous rate of reversal of the changes in the Soret region is similar to that of WT MauG. The much slower reversal of the changes in the NIR region suggests that during the first few minutes after H_2O_2 addition there is a shift to a more stable distribution of resonance structures in which the "true" *bis*-Fe^{IV} state is no longer dominant. This does not affect the reactivity of the *bis*-Fe^{IV} state towards substrates because those catalytic reactions occur prior to this redistribution of resonance structures. The demonstration that multiple amino acid residues in different regions of the diheme site of MauG can influence the distribution of resonance structures that are associated with the *bis*-Fe^{IV} of MauG is intriguing and forms a basis for future studies to fully understand the nature of this charge–resonance-transition phenomenon that allows remarkable stabilization of the high-valent state of the diheme site of MauG.

Transparency document

The Transparency document associated with this article can be found in the online version.

Acknowledgments

This research was supported by the National Institute of General Medical Sciences of the National Institutes of Health under award numbers R37GM41574 (VLD), R01GM66569 (CMW), and Mississippi INBRE, funded by an Institutional Development Award (IDeA) from the National Institute of General Medical Sciences of the National Institutes of Health under grant number P20GM103476 (MF).

Computer resources were provided by the Basic Sciences Computing Laboratory of the University of Minnesota Supercomputing Institute, and we thank Nancy Rowe for her support. X-ray data were collected at the Kahlert Structural Biology Laboratory (KSBL) at The University of Minnesota and GM/CA-CAT at the Advanced Photon Source (APS), Argonne National Laboratory, Argonne, IL. GM/CA CAT has been funded in whole or in part with Federal funds from the National Cancer Institute (Y1-CO-1020) and the National Institute of General Medical Science (Y1-GM-1104). The use of the APS was supported by the U.S. Department of Energy, Basic Energy Sciences, Office of Science, under contract No. DE-AC02-06CH11357. We thank Ed Hoeffner for KSBL support, and the staff at Sector 23, APS for their support. Resonance Raman spectra were collected at the Analytical Core Laboratory (RCMI core facility) at Jackson State University (supported by NIH-RCMI program, grant number 8G12MD007581).

References

[1] V.L. Davidson, Protein-derived cofactors. Expanding the scope of post-translational modifications, Biochemistry 46 (2007) 5283–5292.
[2] V.L. Davidson, Generation of protein-derived redox cofactors by posttranslational modification, Mol. BioSyst. 7 (2011) 29–37.
[3] W.S. McIntire, D.E. Wemmer, A. Chistoserdov, M.E. Lidstrom, A new cofactor in a prokaryotic enzyme: tryptophan tryptophylquinone as the redox prosthetic group in methylamine dehydrogenase, Science 252 (1991) 817–824.
[4] V.L. Davidson, Pyrroloquinoline quinone (PQQ) from methanol dehydrogenase and tryptophan tryptophylquinone (TTQ) from methylamine dehydrogenase, Adv. Protein Chem. 58 (2001) 95–140.
[5] Y. Wang, M.E. Graichen, A. Liu, A.R. Pearson, C.M. Wilmot, V.L. Davidson, MauG, a novel diheme protein required for tryptophan tryptophylquinone biogenesis, Biochemistry 42 (2003) 7318–7325.
[6] A.R. Pearson, T. De La Mora-Rey, M.E. Graichen, Y. Wang, L.H. Jones, S. Marimanikkupam, S.A. Agger, P.A. Grimsrud, V.L. Davidson, C.M. Wilmot, Further insights into quinone cofactor biogenesis: probing the role of mauG in methylamine dehydrogenase tryptophan tryptophylquinone formation, Biochemistry 43 (2004) 5494–5502.
[7] V.L. Davidson, C.M. Wilmot, Posttranslational biosynthesis of the protein-derived cofactor tryptophan tryptophylquinone, Annu. Rev. Biochem. 82 (2013) 531–550.
[8] E.T. Yukl, F. Liu, J. Krzystek, S. Shin, L.M. Jensen, V.L. Davidson, C.M. Wilmot, A. Liu, Diradical intermediate within the context of tryptophan tryptophylquinone biosynthesis, Proc. Natl. Acad. Sci. U. S. A. 110 (2013) 4569–4573.
[9] L.M. Jensen, R. Sanishvili, V.L. Davidson, C.M. Wilmot, In crystallo posttranslational modification within a MauG/pre-methylamine dehydrogenase complex, Science 327 (2010) 1392–1394.
[10] N. Abu Tarboush, L.M.R. Jensen, E.T. Yukl, J. Geng, A. Liu, C.M. Wilmot, V.L. Davidson, Mutagenesis of tryptophan199 suggests that hopping is required for MauG-dependent tryptophan tryptophylquinone biosynthesis, Proc. Natl. Acad. Sci. U. S. A. 108 (2011) 16956–16961.
[11] M. Choi, S. Shin, V.L. Davidson, Characterization of electron tunneling and hole hopping reactions between different forms of MauG and methylamine dehydrogenase within a natural protein complex, Biochemistry 51 (2012) 6942–6949.
[12] S. Shin, V.L. Davidson, MauG, a diheme enzyme that catalyzes tryptophan tryptophylquinone biosynthesis by remote catalysis, Arch. Biochem. Biophys. 544 (2014) 112–118.
[13] C.M. Wilmot, V.L. Davidson, Uncovering novel biochemistry in the mechanism of tryptophan tryptophylquinone cofactor biosynthesis, Curr. Opin. Chem. Biol. 13 (2009) 469–474.
[14] C.W. Wilmot, V.L. Davidson, Uncovering novel biochemistry in the mechanism of tryptophan tryptophylquinone cofactor biosynthesis, Curr. Opin. Chem. Biol. 13 (2009) 462–467.
[15] X. Li, R. Fu, S. Lee, C. Krebs, V.L. Davidson, A. Liu, A catalytic di-heme bis-Fe(IV) intermediate, alternative to an Fe(IV)═O porphyrin radical, Proc. Natl. Acad. Sci. U. S. A. 105 (2008) 8597–8600.
[16] J. Geng, K. Dornevil, V.L. Davidson, A. Liu, Tryptophan-mediated charge–resonance stabilization in the bis-Fe(IV) redox state of MauG, Proc. Natl. Acad. Sci. U. S. A. 110 (2013) 9639–9644.
[17] N. Abu Tarboush, L.M. Jensen, M. Feng, H. Tachikawa, C.M. Wilmot, V.L. Davidson, Functional importance of tyrosine 294 and the catalytic selectivity for the bis-Fe(IV) state of MauG revealed by replacement of this axial heme ligand with histidine, Biochemistry 49 (2010) 9783–9791.
[18] N. Abu Tarboush, S. Shin, J. Geng, A. Liu, V.L. Davidson, Effects of the loss of the axial tyrosine ligand of the low-spin heme of MauG on its physical properties and reactivity, FEBS Lett. 586 (2012) 4339–4343.
[19] L.M. Jensen, Y.T. Meharenna, V.L. Davidson, T.L. Poulos, B. Hedman, C.M. Wilmot, R. Sarangi, Geometric and electronic structures of the His–Fe(IV)═O and His–Fe(IV)–Tyr hemes of MauG, J. Biol. Inorg. Chem. 17 (2012) 1241–1255.
[20] Y. Ling, V.L. Davidson, Y. Zhang, Unprecedented Fe(IV) species in a diheme protein MauG: a quantum chemical investigation on the unusual Mossbauer spectroscopic properties, J. Phys. Chem. Lett. 1 (2010) 2936–2939.
[21] S. Shin, M. Feng, V.L. Davidson, Mutation of Trp(93) of MauG to tyrosine causes loss of bound Ca(2+) and alters the kinetic mechanism of tryptophan tryptophylquinone cofactor biosynthesis, Biochem. J. 456 (2013) 129–137.
[22] M. Feng, L.M. Jensen, E.T. Yukl, X. Wei, A. Liu, C.M. Wilmot, V.L. Davidson, Proline 107 is a major determinant in maintaining the structure of the distal pocket and reactivity of the high-spin heme of MauG, Biochemistry 51 (2012) 1598–1606.
[23] E.T. Yukl, H.R. Williamson, L. Higgins, V.L. Davidson, C.M. Wilmot, Oxidative damage in MauG: implications for the control of high-valent iron species and radical propagation pathways, Biochemistry 52 (2013) 9447–9455.

[24] S. Shin, E.T. Yukl, E. Sehanobish, C.M. Wilmot, V.L. Davidson, Site-directed mutagenesis of Gln103 reveals the influence of this residue on the redox properties and stability of MauG, Biochemistry 53 (2014) 1342–1349.
[25] N. Abu Tarboush, E.T. Yukl, S. Shin, M. Feng, C.M. Wilmot, V.L. Davidson, Carboxyl group of Glu113 is required for stabilization of the diferrous and bis-Fe(IV) states of MauG, Biochemistry 52 (2013) 6358–6367.
[26] X. Li, M. Feng, Y. Wang, H. Tachikawa, V.L. Davidson, Evidence for redox cooperativity between *c*-type hemes of MauG which is likely coupled to oxygen activation during tryptophan tryptophylquinone biosynthesis, Biochemistry 45 (2006) 821–828.
[27] S. Lee, S. Shin, X. Li, V. Davidson, Kinetic mechanism for the initial steps in MauG-dependent tryptophan tryptophylquinone biosynthesis, Biochemistry 48 (2009) 2442–2447.
[28] W. Kabsch, Xds, Acta Crystallogr. D Biol. Crystallogr. 66 (2010) 125–132.
[29] G.N. Murshudov, A.A. Vagin, E.J. Dodson, Refinement of macromolecular structures by the maximum-likelihood method, Acta Crystallogr. D Biol. Crystallogr. 53 (1997) 240–255.
[30] CCP4, Collaborative Computational Project Number 4, Acta Crystallogr. Sect. D: Biol. Crystallogr. 50 (1994) 760–763.
[31] P. Emsley, K. Cowtan, Coot: model-building tools for molecular graphics, Acta Crystallogr. D Biol. Crystallogr. 60 (2004) 2126–2132.
[32] S. Hu, I.K. Morris, J.P. Singh, K.M. Smith, T.G. Spiro, Complete assignment of cytochrome *c* resonance raman spectra via enzymatic reconstitution with isotopically labeled heme, J. Am. Chem. Soc. 115 (1993) 12446–12458.
[33] A.T. Tu, Raman Spectroscopy in Biology; Principles and Applications, John Wiley and Sons Inc., New York 1982, pp. 331–337.
[34] A. Desbois, Resonance Raman spectroscopy of *c*-type cytochromes, Biochimie 76 (1994) 693–707.
[35] S. Shin, N. Abu Tarboush, V.L. Davidson, Long range electron transfer reactions between hemes of MauG and different forms of tryptophan tryptophylquinone of methylamine dehydrogenase, Biochemistry 49 (2010) 5810–5816.
[36] S. Shin, V.L. Davidson, MauG, a diheme enzyme that catalyzes tryptophan tryptophylquinone biosynthesis by remote catalysis, Arch. Biochem. Biophys. 544 (2014) 112–118.